Chapter 4

Explainable Neural Network Architecture for Battery Health Estimation

The operational safety of lithium-ion batteries is heavily dependent on accurate battery state of health (SOH) assessments. This chapter introduces a novel hybrid algorithm: a multi-faceted temporal convolutional network with dynamic weight adaptation (MFDWA) combined with a gated recurrent unit (GRU) to estimate the SOH of lithium-ion batteries across various experimental setups. The MFDWA architecture includes multiple temporal convolutional network (TCN) branches, each containing a dilated TCN block, attention blocks, and dynamic weight adaptation components. This multi-branch structure captures multiscale patterns through different dilation rates, while attention blocks select essential input features. The dynamic weight adaptation mechanism further enhances performance by addressing evolving battery dynamics. The GRU component tracks temporal information sequences by retaining relevant past states. The proposed hybrid algorithm performs better than the existing state-of-the-art methods, achieving lower mean absolute error (MAE) and root mean square error (RMSE) values across multiple datasets while maintaining parameter compatibility. These results indicate the model's robustness across different initial conditions, battery combinations, and varying

prediction horizons. Additionally, the integration of explainable artificial intelligence (XAI) through the SHapley Additive exPlanations (SHAP) technique in the proposed hybrid model prioritizes input features, improves model performance, and enhances interpretability, thus fostering user trust.

4.1 Introduction

The transition toward sustainable energy and transportation has intensified the focus on lithium-ion batteries (LIBs), which are widely adopted in electric vehicles (EVs) and renewable energy storage systems. Their high energy density, long cycle life, and efficiency make them the preferred choice over other storage technologies. However, the performance and safety of LIBs inevitably degrade over time due to aging and usage, necessitating reliable indicators to assess their condition. Among these, the state of health (SOH) has become a critical metric, providing a quantitative measure of a battery's remaining capacity and power capability relative to its initial state.

The widely used approaches for SOH estimation in batteries are direct measurement methods, model-based methods and data-centric methods [133]. Direct measurement methods such as coulomb count and open circuit voltage are based on observable and measurable quantities that correlate with battery health status [134]. These methods require more time for experimentation and are primarily limited to lab-based studies. Model-based approaches seek to develop mathematical representations describing LIBs' deterioration, such as electrochemical models, particle filters, and Kalman filters [135]. The predictive accuracy of the model-based method relies on predefined models, and these models struggle to handle sophisticated and non-linear trends in battery degradation mechanisms. Model-based approaches are also computationally demanding due to their iterative and probabilistic nature. A data-centric approach is wholly dependent on the extensive availability of data. The extensive use of numerous sensors makes ample data readily accessible for data-driven methods. Like model-based methods, data-driven

approaches do not necessitate understanding battery degradation mechanisms [95]. They adeptly manage batteries' nonlinear and intricate behavior through robust learning and data mining capabilities [136].

Data-centric strategies for predicting the health of batteries are classified into machine learning-based, deep learning-based, and hybrid approaches [137]. Machine learning algorithms establish connections between historical data and anticipated SOH through diverse models. Battery attributes such as voltage, current, temperature, and charging-discharging cycles change over time, making them inherently time-dependent [138]. Deep learning methods are a popular choice for forecasting battery life due to their intrinsic feature extraction capabilities, ability to manage enormous volumes of time-dependent data, and understanding of complex patterns in degradation mechanisms [139]. The recurrent neural network (RNN) is a subcategory of deep learning that can effectively predict the current output values using historical and present battery data available [116]. These RNN models effectively handle time-variant features in LIB data. However, conventional RNN architectures suffer from the vanishing gradient issue in the presence of long-range dependencies in battery data. This challenge is surmounted by RNN models such as long short-term memory (LSTM), and gated recurrent unit (GRU) that incorporate a gated structure [140]. In understanding how battery degradation occurs over a more extended period, GRU is preferred over LSTM because of its sleek design, faster speed, and less storage space.

SOH prediction uses deep learning models like convolutional neural networks (CNNs) because they are good at hierarchical feature extraction from the given spatial data [141]. Despite their advantages, CNN has a major drawback in processing battery data with long-range temporal dependencies. Advanced deep learning systems are the widely preferred choice in SOH prediction due to their ability to handle sophisticated trends in battery data. Transformer architecture and its variants [142], [82] effectively capture long-range dependencies with their attention blocks. These architectures provide robust

temporal modeling and good interpretability of results. The major drawback of these transformer-based models is that they require large-scale datasets for better performance, and they are computationally complex models. The graph neural network (GNN) is an advanced SOH estimation technique employed in battery packs that captures both the spatial and temporal information across cells within the battery pack [143], [144]. These GNN models are not suited for cell-level estimation and face oversmoothing issues with shallow graph structures.

Physics-informed neural networks are gaining popularity in battery degradation tasks by using the advantages of both data-driven techniques and electrochemical theory [145]. These techniques require prior domain knowledge and are inherently complex to be implemented in real-time battery applications. Hybrid models based on TCN, CNN, or LSTM architectures, as seen in [146], [147] are designed to capture spatial and temporal trends in battery degradation data. These hybrid models follow static architectures using fixed feature fusion strategies and don't dynamically prioritise features pertinent to the degradation of the LIB. Temporal convolutional networks (TCNs) are more appropriate for applications involving sequences because they manage to preserve and exploit the long-range temporal dependencies of the battery data [148]. Nonetheless, additional network-tuning or a hybrid technique may be required to model complicated degradation characteristics over extended timescales.

Existing SOH estimation methods face challenges in balancing accuracy, efficiency, and robustness, particularly for batteries with complex, long-term degradation behaviors. The major research gaps identified in the existing techniques for SOH estimation are:

- Lack of dynamic adaptation: The existing deep learning techniques fail to adapt to dynamically evolving changes in battery degradation over time. These static architectures don't work well in aged batteries as degradation evolves over time.
- Capturing multi-scale temporal dependencies: The existing TCN architectures work well with fixed dilation rates. The models fail to learn multiscale patterns that

could capture short-term fluctuation and long-term trends in battery deterioration.

- Computational complexity in transformer models: Transformer-based models work well in SOH estimation techniques, but they are computationally complex and fail to capture degradation patterns in limited data, or small datasets.
- Temporal modeling issue in RNN/CNN: RNN models face the issue of vanishing gradients while dealing with long-term dependencies in degradation data; meanwhile, CNN architecture extracts spatial features, but fails to understand the temporal trends in battery data.
- Uniform weighting of features and temporal scales: Existing techniques treat input and time steps evenly, ignoring the reality that specific information becomes more important as the battery ages

To resolve the aforementioned issues, an advanced approach is required that integrates multi-branch TCNs with diverse dilation rates, attention mechanisms to prioritise critical features, and dynamic weight adaptation to effectively handle evolving degradation dynamics. To address these limitations, this chapter proposes a novel multi-faceted temporal convolutional network with dynamic weight adaptation (MFDWA) to tackle the challenges of modeling complex battery degradation over long time series.

The novel MFDWA architecture contains multiple branches with attention blocks, dynamic weight adaptation, and a TCN block with sequential dilated convolution layers. These varying dilation rates in the TCN block help to capture multi-scale dependencies within the degradation of the LIB data. The MFDWA architecture features several branches, each containing a TCN block with varying dilation rates. These blocks capture short-term, medium-term, and long-term dependencies in battery degradation patterns. Additionally, dynamic weight adaptation and attention mechanisms are employed to prioritize relevant features and adjust the contribution of each branch based on evolving battery conditions, improving model performance. The resulting outputs of the branches are concatenated, with residual connections added to preserve the input before passing

through a GRU layer. The extracted features are then fed to the GRU, which uses its gating mechanism to capture long-range dependencies and learn temporal patterns over extended periods.

Hybrid approaches that use machine learning and deep learning models dominate over simpler models due to their ability to combine the benefits of several models, thus enhancing the strength and predictive power of the model [149], [150]. The integration of GRU into the novel MFDWA architecture is essential for further improving SOH predictions. MFDWA's multi-branch structure encodes complex degradation patterns, while GRU's ability to learn sequential dependencies and adapt to evolving battery behavior ensures enhanced reliability and accuracy for extended SOH forecasting. Incorporating explainable artificial intelligence (XAI) techniques, such as SHapley Additive exPlanations (SHAP), into the proposed model allows users and developers to gain deeper insights into the critical input features influencing RUL prediction. This transparency not only improves model performance through effective feature selection but also boosts user confidence by making the decision-making process of the model more interpretable and understandable.

The major contributions of this chapter are:

- Integrating MFDWA with GRU enables the model to capture evolving battery behavior over extended periods. MFDWA extracts short-term fluctuations and long-term aging patterns, while GRU dynamically adapts to shifting degradation trends, significantly boosting the accuracy and robustness of SOH prediction.
- An innovative early-stage SOH prediction framework that leverages MFDWA's multi-scale temporal feature extraction to accurately forecast battery degradation from minimal capacity fade data, overcoming the limitation of existing methods that require extensive degradation history for reliable predictions.
- A memory-efficient deep learning architecture that achieves state-of-the-art SOH prediction performance with significantly lower mean absolute error (MAE) and

root mean square error (RMSE) values compared to existing methods across heterogeneous battery datasets. This is achieved through MFDWA's dynamic weight adaptation mechanisms, which learn evolving degradation patterns over time and adaptively allocate computational resources, enabling deployment in resource-constrained battery management systems.

- The utilization of the XAI technique SHAP in the proposed model enhances the transparency and interpretability of the model in predicting the RUL of the battery. This integration facilitates the recognition of crucial input features during the data processing stage and offers an understanding of their respective impacts on the prediction process, promoting trust among users and developers.

4.2 Proposed Methodology

The proposed MFDWA architecture contains multi-branch TCNs, with each branch containing: (a) an attention mechanism, (b) a single TCN block with N_b sequential dilated convolution layers, and (c) dynamic weight adaptation, as shown in Fig. 4.1. The multi-faceted architecture of TCN contains multiple branches operating independently in parallel. Unlike conventional TCN-based approaches, the proposed architecture introduces a novel cross-adaptive attention mechanism that dynamically reweights each branch based on its contribution to SOH prediction, ensuring optimal feature extraction. Each branch has an attention mechanism to select the most pertinent data from the input data for SOH estimation. The network takes as sequential input $x_{t,i,k}$, where i is the sample index, t is the index of the time step, and k stands for the feature index. The attention applied to the relevant branch at time t is given by the following equation:

$$A_{b,t} = \text{Softmax}\left(\frac{Q_b \cdot K_b^T}{\sqrt{d_k}} + Bi_b\right) \tag{4.1}$$

$A_{b,t}$ denotes the weight of attention at time step t for branch b, the softmax is an activation function for normalizing the attention scores, where b is the number of branches used, d_k represents the key vectors and query's dimensionality, where k denotes the dimension unique to the attention mechanism. Q_b is the query vector for branch b, K_b is the key vector for branch b, and Bi_b is the bias term used for the attention. The attention is then applied to the input data X_t. The input $X_{b,t}$ for the branch b at time t, modulated by the attention weight, is given by:

$$X_{b,t} = A_{b,t} \cdot X_t \tag{4.2}$$

This modulation adjusts the input X_t by the attention weights, focusing on the most important input data for each branch. These branches in the multi-faceted TCN contain TCN block with each branch containing: (a) an attention block, (b) a single TCN block with N_b sequential dilated convolution layers, and (c) dynamic weight adaptation. A key novelty lies in the strategic deployment of varying dilation rates across branches, enhancing the model's ability to capture multi-scale dependencies that vary from short-term degradation patterns to long-term battery health trends. For each layer n in branch b, the output of the dilated convolution is computed as follows:

$$Y_{b,n,t} = \text{ReLU}\left(\sum_{i=1}^{K} W_{b,n,i} \cdot X_{b,t-i\cdot D_{b,n}} + Bi_{b,n}\right) \tag{4.3}$$

where $W_{b,n,i}$ is the weight matrix for filter i in branch b at layer n, $D_{b,n}$ is the dilation factor for layer n in branch b, $Bi_{b,n}$ is the bias term for the n-th layer in branch b, N_b is the number of dilated layers in branch b, and K is the kernel size. The accumulated branch output $F_{b,t}$ for branch b is

$$F_{b,t} = \sum_{n=1}^{N_b} Y_{b,n,t} \tag{4.4}$$

Algorithm 2 MFDWA Algorithm

Input: Sequential data $X = x_{itk}$, where i is the sample index, t represents the time steps, and k denotes the feature dimensions.

Initialization: Define parameters:

- B: Number of branches.
- N_b: Number of dilated convolution layers in each branch.
- $D_{b,n}$: Dilation rates for each layer in each branch.
- K: Kernel size.
- λ: Weight adaptation factor.
- Q_b: Query matrix for attention in branch b.
- K_b: Key matrix for attention in branch b.
- d_k: Dimensionality of the key vectors.
- Bi_b: Bias term for attention in branch b.

MFDWA Operations:

for $t = 1$ to T **do**
  Initialize $F_t = 0$
  /Initialize fused output for time step t.
  for $b = 1$ to B **do**
    Initialize $F_{b,t} = 0$
    /Initialize branch output for time step t.
    (a) Attention mechanism
    Compute attention weight $A_{b,t}$:
    $A_{b,t} = \text{Softmax}\left(\frac{Q_b \cdot K_b^\top}{\sqrt{d_k}} + Bi_b\right)$
    */*Compute attention weight for branch b at time step t.*
    Apply attention to input:
    $X_{b,t} = A_{b,t} \cdot X_t$
    */*Modulate the input sequence using the computed attention weight.*
    (b) TCN block with N_b sequential dilated convolution layers
    for $n = 1$ to N_b **do**
      Compute the output of the dilated convolution layer:
      $Y_{b,n,t} = \text{ReLU}\left(\sum_{i=1}^{K} W_{b,n,i} \cdot X_{b,t-i \cdot D_{b,n}} + Bi_{b,n}\right)$
      */*Compute output of the n^{th} dilated convolution layer in branch b at time step t.*
      Update the branch output for time step t:
      $F_{b,t} = F_{b,t} + Y_{b,n,t}$
      */*Accumulate the output of the n^{th} layer in branch b at time step t.*
    end for
    (c) Dynamic weight adaptation
    Apply dynamic weight adaptation:
    $F_{b,t} = \lambda_b \cdot F_{b,t}$
    */*Adjust the accumulated output for each branch using dynamic weight adaptation.*
    Add branch output to fused output:
    $F_t = F_t + F_{b,t}$
    */*Accumulate the output from branch b to the fused output.*
  end for
  Apply residual connection:
  $F_t = F_t + X_t$
  */*Add residual connection with original input.*
  Normalize the fused output:
  $F_t = \text{LayerNorm}(F_t)$
  */*Apply layer normalization to the fused output.*
end for

Output: Fused representation F_t capturing diverse temporal patterns across all branches for each time step, enhanced with attention and dynamic weight adaptation.

This equation accumulates the results of the dilated convolution across all the

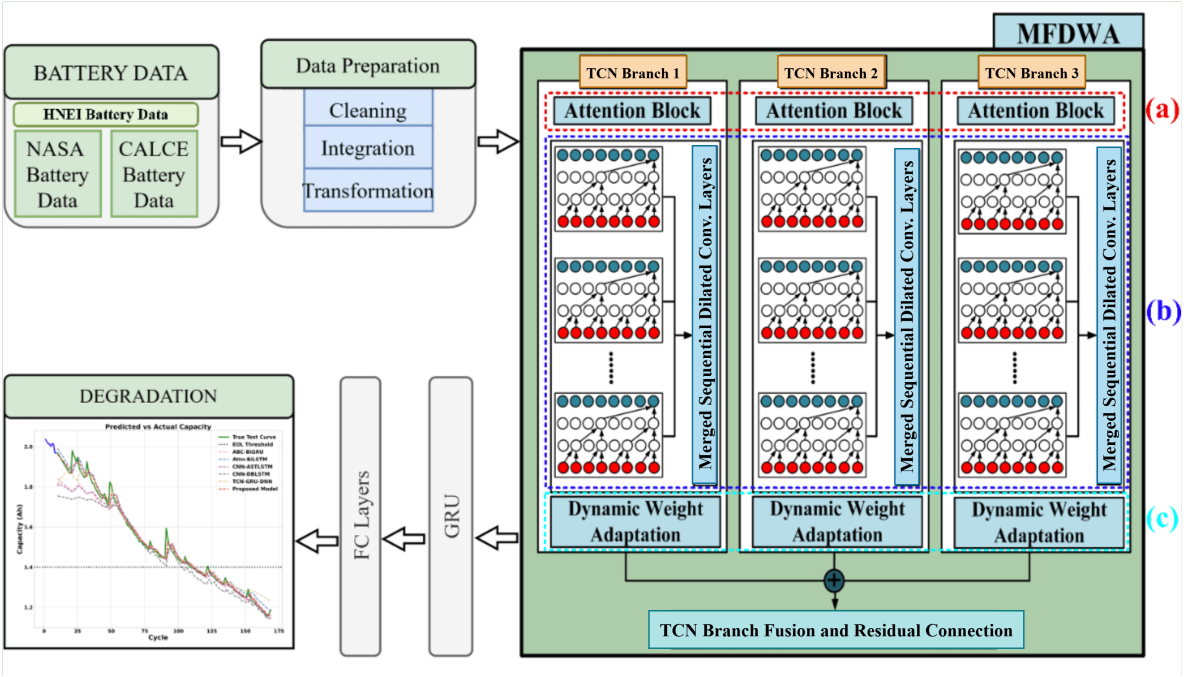

Figure 4.1: MFDWA-GRU model for SOH estimation.

dilated convolution layers in branch b. In the above multifaceted architecture, each branch operates independently. The importance of each branch in TCN varies, with some branches contributing more importance to life prediction. The novelty is further enhanced by a dynamic weight adaptation strategy, where the model autonomously learns the significance of each branch based on real-time performance. Dynamic weight adaptation is employed for each branch, which assigns a learnable weight for individual branches, which in turn adjusts the contribution of the branches to the final output capacitance prediction dynamically.

$$F_{b,t} = \lambda_b \cdot F_{b,t} \tag{4.5}$$

where λ_b is the learnable weight adaptation factor for branch b. The fused output F_t at time step t is a combination of all branch outputs and the original input:

$$F_t = \sum_{b=1}^{B} F_{b,t} + X_t \tag{4.6}$$

This is where all the branch outputs come together to form the final fused output F_t at time step t. This equation signifies the combination of outputs from all branches of the model along with the input X_t. The addition of the input to the aggregated branch outputs implements a residual connection. Finally, the fused output is normalized using layered normalization. The final output F_t represents the fused and normalized temporal representation after all operations:

$$F_t = \text{LayerNorm}\left(\sum_{b=1}^{B} \lambda_b \cdot \left(\sum_{n=1}^{N_b} \text{ReLU}\left(\sum_{i=1}^{K} W_{b,n,i} \cdot X_{b,t-i\cdot D_{b,n}} + Bi_{b,n}\right)\right) + X_t\right) \quad (4.7)$$

The entire steps of the novel MFDWA architecture are detailed in Algorithm 2. The second component of the model is the GRU operating in conjunction with the MFDWA algorithm. The normalized fused output from MFDWA is passed to the GRU, effectively capturing the sequential and temporal dependencies in battery data. The output of GRU is passed to a set of dense layers with a final dense layer to predict the capacitance degradation of the battery. The entire framework of the proposed hybrid model for health estimation is shown in Fig. 4.1. The parameters of the model are optimized using hyperband optimization. The optimized parameters are as follows: the MFDWA operates with three TCN branches, each utilizing 32 filters and a kernel size of 3, followed by a GRU with 64 units and three dense layers with 32, 16, and 1 units, respectively. LIB battery degradation in a real-world scenario is nonlinear and dynamic in nature, concerning charge-discharge cycles, operating temperature, and usage trends. This inconsistency in degradation can be handled by the multi-branch architecture of MFDWA. This multi-branch TCN, with its varying dilation rates, understand the degradation pattern at different temporal resolutions at the same time. The branches with short-term dependencies capture the sudden fluctuations arising from the charge-discharge cycle, and branches with long-term dependencies can focus on capacity fade and rise in internal resistance. The dynamic weight adaptation module in MFDWA

helps the model adapt to the continuously evolving nature of battery degradation. These dynamic weights assigned at different stages of degradation (early, mid and later) increase the robustness of the proposed model, guaranteeing a reliable SOH estimation technique even in non-uniform degradation trends.

In the proposed architecture, dynamic weight adaptation is applied after each TCN branch to modulate the contribution of each temporal feature map before combining them. Specifically, a learnable weight is computed for each feature map using a dense layer with a sigmoid activation, which outputs a value between 0 and 1. This weight is then element-wise multiplied with the corresponding feature map, effectively scaling its contribution based on its importance. During training, these weights are learned jointly with the network parameters via backpropagation, allowing the model to automatically emphasize relevant temporal patterns and suppress less informative ones. This adaptive mechanism enhances the model's ability to capture critical degradation trends and improves the overall SOC prediction accuracy, particularly under varying operating conditions.

4.3 Results and Discussion

4.3.1 Dataset Description and Experimental setup

The primary dataset used in the proposed work is obtained from the Hawaii Natural Energy Institute (HNEI), which consists of fourteen Nickel Manganese Cobalt Oxide-Lithium Cobalt Oxide 18650 batteries, each with a rated capacity of 2.8 Ah. Over 1,000 cycles at 25°C, the batteries charged at a pace of C/2 followed by a discharge speed of 1.5 C. Data from these cycles were analyzed to extract features depicting voltage and current behavior. Key characteristics considered for prediction in the dataset included cycle index, discharge time, time taken to reach 4.15V, time under constant current, duration between voltage decrements from 3.6V to 3.4V, maximum discharge voltage,

Table 4.1: Performance comparison with the state-of-the-art models on the HNEI Dataset.

Methodology	MAE%	RMSE%	Parameters	Train Time (s)	Infer Time (s)	Memory(KB)
Attention-BiLSTM [151]	17.76	26.42	78145	580.06	2.64	305.25
TCN-GRU-DNN-Attention [152]	11.70	15.94	42369	1453.64	2.69	165.50
CNN-LSTM-DNN [153]	13.58	18.37	62337	**467.71**	1.35	243.51
BiGRU-Transformer [154]	7.69	10.23	71745	1409.77	2.91	280.25
Attentive-LSTM [155]	8.69	11.79	49969	545.54	**0.72**	195.19
CNN-MMHA [156]	6.57	9.10	200723	1392.82	1.57	784.07
MFDWA-GRU (Proposed)	**6.29**	**8.76**	**33904**	1350.21	1.88	**132.44**

minimum charge voltage, and charging duration. The feature cycle index is not used for life estimation because its value directly correlates with the battery life. The life of the battery is estimated in days for each of the fourteen batteries using these input features.

The secondary dataset captures the degradation patterns of LIBs provided by the NASA Prognostics Center of Excellence (PCoE). These batteries operate at ambient temperature under different processes, such as charging, discharging, and impedance measurements. The dataset includes data from four LIBs (B005, B006, B007, and B0018) with a rated capacity of 2 Ah measured by built-in sensors. The third data set includes four battery samples; CS2-35, CS2-36, CS2-37, and CS2-38 provided by the CALCE lab at the University of Maryland. Each battery was charged using a standard constant current/constant voltage (CC-CV) method. They were first charged at a steady 0.5C current until reaching 4.2V. After that, the voltage was held at 4.2V while the current slowly dropped, stopping once it fell below 0.05A. For discharging, the batteries ran until they hit a cut-off voltage of 2.7V. The data for the CS2 cells was collected using battery testers equipped with built-in sensors to track key measurements like voltage, current, and temperature.

The life of the battery is defined as the number of cycles required for the battery to reach its end of life, which is determined when its rated capacity falls below 70% of its total capacity in the NASA dataset and 80% of its total capacity in the CALCE dataset

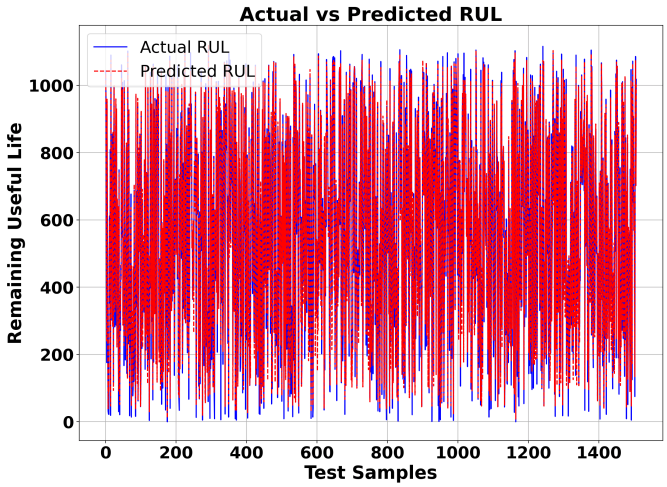

Figure 4.2: Predicted vs Actual Useful Life – HNEI Dataset.

[153]. SOH can be defined using the value of the capacity as:

$$\text{SOH} = \frac{Q_{\text{meas}}}{Q_{\text{rated}}} \tag{4.8}$$

where Q_{meas} is the current measured capacity, and Q_{rated} is the rated capacity of the new battery The previous capacity values were used as input in the experiments, while the current capacity is the predicted output [151].

The proposed model was trained within a Windows 11 environment, utilizing an Intel i7-10510U CPU operating at 1.80 GHz. A software stack consisting of Python version 3.11.0, TensorFlow, Keras, and Jupyter Lab was employed to establish a robust framework for machine learning and deep learning analysis and experimentation. Performance evaluation of the model utilized MAE, RMSE, and R2 scores as error metrics.

4.3.2 Comparison with existing techniques for life prediction

The effectiveness of the proposed hybrid model for estimating battery life was thoroughly evaluated by comparing it against an array of advanced hybrid machine learning and deep learning algorithms. The state-of-the-art models include TCN-LSTM, Attention-

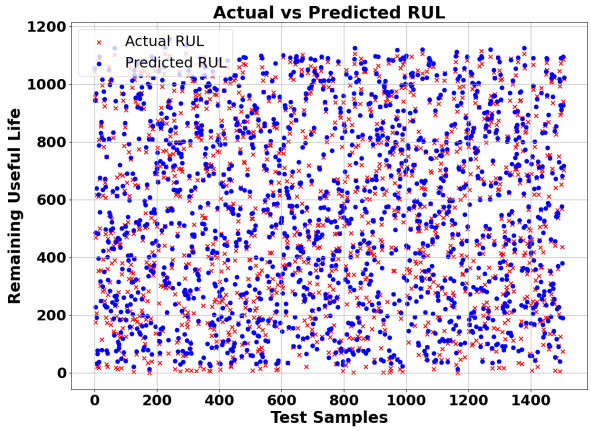

Figure 4.3: Scatter Plot of Actual vs. Predicted RUL Values.

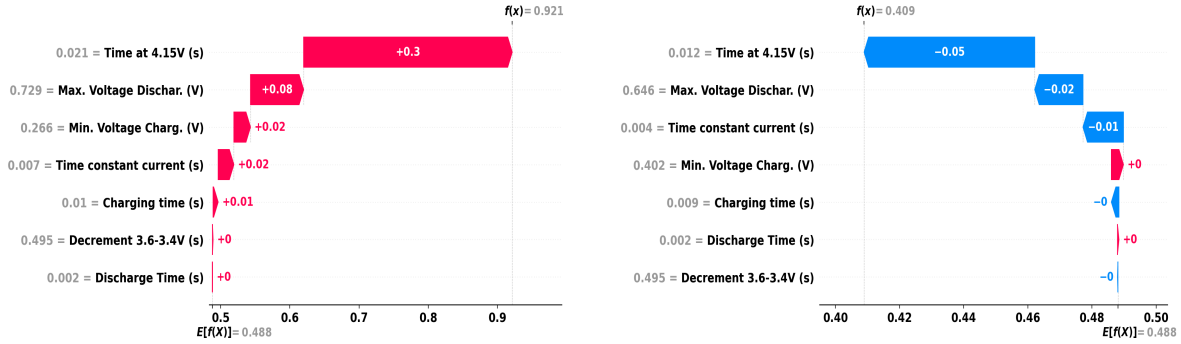

(a) (b)

Figure 4.4: Feature importance for individual instances using SHAP (a) Instance no 72 (b) Instance no 143.

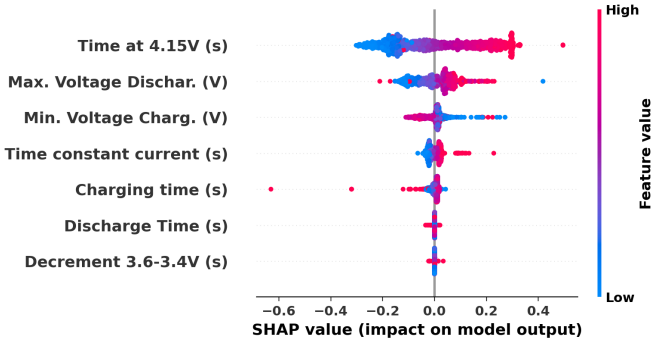

Figure 4.5: Summary plot for all test instances of battery data using SHAP.

Bidirectional LSTM (Attention-BiLSTM), Bidirectional GRU-Transformer (BiGRU-Transformer), CNN-LSTM-deep neural network (CNN-LSTM-DNN), and TCN-GRU-DNN with dual attention, a machine learning algorithm using random forest, attentive-LSTM, and CNN-Mask Multi-Head Attention Mechanisms (CNN-MMHA). Through comprehensive analysis, it was found that the proposed hybrid model exhibited better performance in terms of RMSE, MAE, and R2-score, showcasing its effectiveness in life estimation over its counterparts in the HNEI dataset, as shown in Table 4.1. All the models used in the comparison were trained using 90% of the dataset, with the remaining 10% reserved for testing. Furthermore, the training set was internally split into 90% for actual training and 10% for validation. In Fig. 4.2, actual RUL represents the true remaining useful life of the battery in terms of the number of days for individual instances. It indicates the number of days the battery effectively functions before it reaches its end of life. Predicted RUL is the RUL predicted by the proposed model, which is recorded in days for individual instances.

The scatter plot in Fig. 4.3 shows a significant alignment between real and predicted RUL values across test samples, implying that the model accurately reflects the battery deterioration trend. The model requires significantly fewer parameters than state-of-the-art models, achieving better results with only 33,904 parameters for the HNEI dataset. With this parameter efficiency, the MFDWA-GRU model performs better than other models in the HNEI dataset with an MAE% of 6.29 and RMSE% of 8.76. The proposed MFDWA-GRU model achieves an inference time of 1.88 seconds in the HNEI dataset, although it's not the fastest among all the models. Moreover, the proposed model is memory efficient with a requirement of 132.44 KB, which is the least among the other models. In addition, the model has moderate training time, and the parameter count is the least compared to other models. The MFDWA-GRU model offers the optimal memory-performance trade-off, striking a balance between inference speed and memory utilisation, making it suitable for resource-constrained environments. The graph showing

the predicted and actual life of the battery using the proposed model within the HNEI dataset for the test instances is shown in Fig. 4.2.

Table 4.2: Battery configuration for experimental scenarios.

Experimental Scenario	Training battery ID	Test battery 1D	Starting point of prediction (% of cycles)
Scenario 1A	B5,B6,B7	B18	5
Scenario 1 B	B5,B6,B7	B18	30
Scenario 1C	B5,B6,B7	B18	50
Scenario 2A	B5,B6,B18	B7	5
Scenario 2B	B5,B6,B18	B7	30
Scenario 2C	B5,B6,B18	B7	50
Scenario 3A	B5,B7,B18	B6	5
Scenario 3B	B5,B7,B18	B6	30
Scenario 3C	B5,B7,B18	B6	50
Scenario 4A	CS35,CS36,CS37	CS38	5
Scenario 4B	CS35,CS36,CS37	CS38	30
Scenario 4C	CS35,CS36,CS37	CS38	50
Scenario 5A	CS35,CS36,CS38	CS37	5
Scenario 5B	CS35,CS36,CS38	CS37	30
Scenario 5C	CS35,CS36,CS38	CS37	50
Scenario 6A	CS5,CS37,CS38	CS36	5
Scenario 6B	CS5,CS37,CS38	CS36	30
Scenario 6C	CS5,CS37,CS38	CS36	50

4.3.3 XAI for feature selection and interpretability

The challenge of transparency in AI models and their applications remains a significant obstacle for developers and users. XAI addresses this challenge by providing understandable explanations for the decisions and predictions made by AI models, aiming to improve understanding and communication between human users and AI systems. Specifically, the XAI method, known as SHAP, enhances the interpretability of life prediction for batteries. Within the proposed hybrid model, the SHAP waterfall plot is utilized to provide insights into individual predictions. These predictions reveal that the importance of features varies across different instances (instance no 72 and instance no 143), as depicted in Fig. 4.4. E[f(x)] is the average predicted value over all instances, while f(x) represents the predicted value of that particular occurrence in each of these individual predictions. Positive values show an increase in the model's forecast from the base value, while negative values show a decrease in the model's predictions. SHAP

Table 4.3: Model Memory and Computational Metrics for SOH Estimation in NASA and CALCE datasets.

Methodology	**Memory Requirement (MB)**	**Avg.Train Time (s)**	**Avg.Infer Time (s)**
ABC-BiGRU [129]	41.402	18.48	0.0579
Attention-BiLSTM [151]	142.711	43.95	0.1143
TCN-GRU-DNN [152]	66.465	91.39	0.0853
CNN-ASTLSTM [157]	23.473	17.42	0.0490
CNN-DBLSTM [158]	209.831	227.84	0.0221
Proposed	66.316	71.85	0.0618

waterfall plots for two specific instances illustrate how individual feature contributions lead to the final prediction in each case. This instance-level interpretability is useful for understanding the model's decision process for specific samples, aiding in debugging and targeted decision-making. In instances 72 and 143, the discharge time and duration between voltage decrements from 3.6V to 3.4V don't contribute to the model prediction.

A summary plot addresses the issues by providing a holistic view of the most influential features within the proposed model. By employing the SHAP technique, summary plots effectively showcase the importance of features across all the individual predictions. In these plots, the distribution of red and blue dots indicates the impact of features on the output: a surplus of red dots on the right suggests a positive impact with higher values. In comparison, a prevalence of blue dots on the left signifies a negative effect with lower values. Fig. 4.5 shows a summary plot highlighting the most influential features in predicting the life of LIBs. It is clear from the summary plots as well as the individual plots, the features such as discharge time and duration between voltage decrements from 3.6V to 3.4V don't contribute significantly to the life estimation within battery data. This summary plots ranks features based on their mean SHAP value and shows the distribution of their impact across all instances. This offers a global view of feature importance and helps identify which features consistently influence the model's predictions. The key contributions of integrating XAI in the proposed model

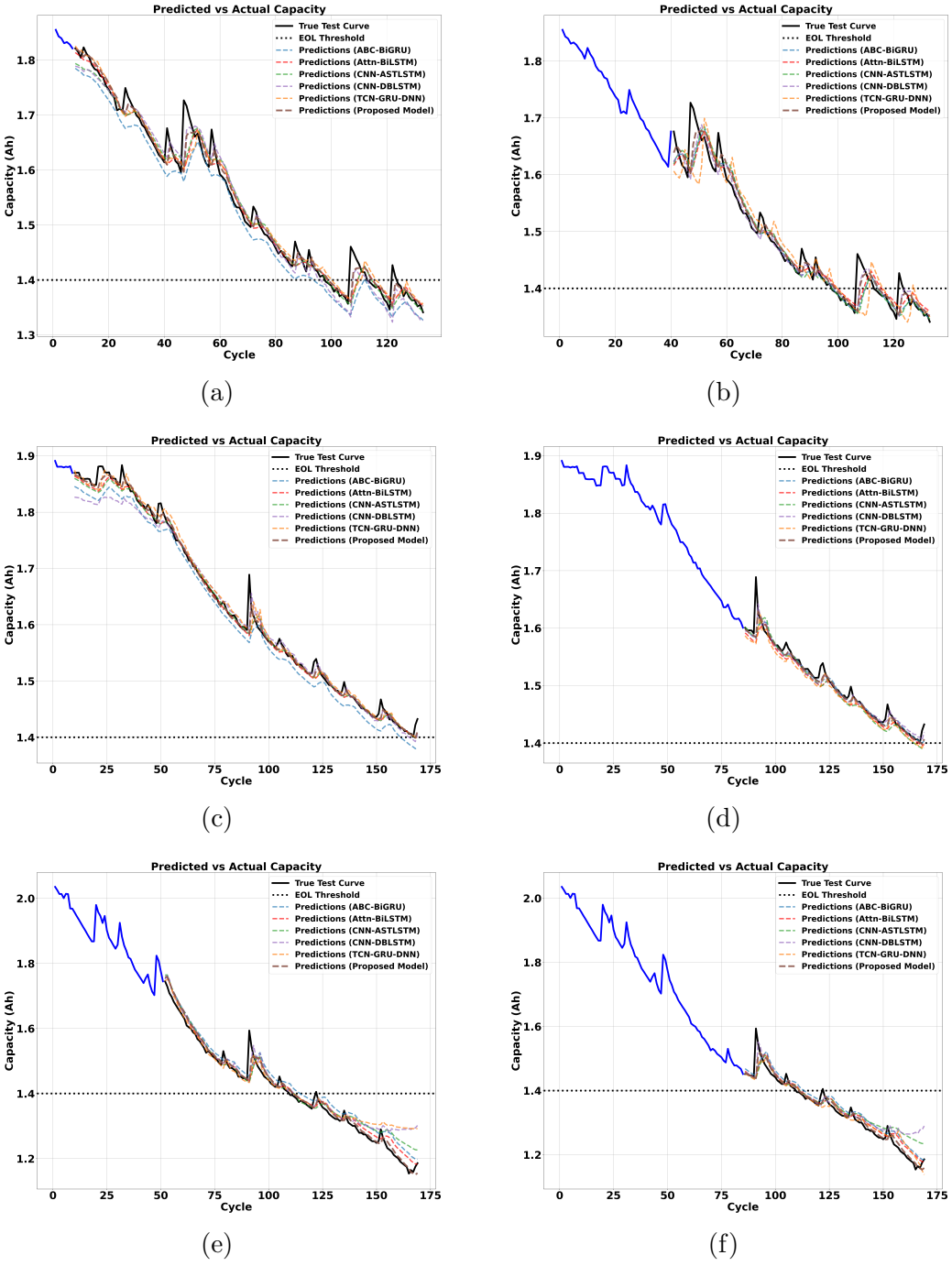

Figure 4.6: Degradation prediction scenarios in NASA dataset (a) Scenario 1A (b) Scenario 1B (c) Scenario 2A (d) Scenario 2C (e) Scenario 3B (f) Scenario 3C.

include improved model transparency, feature importance analysis, error diagnosis and debugging, and enhanced trust and reliability among users and developers.

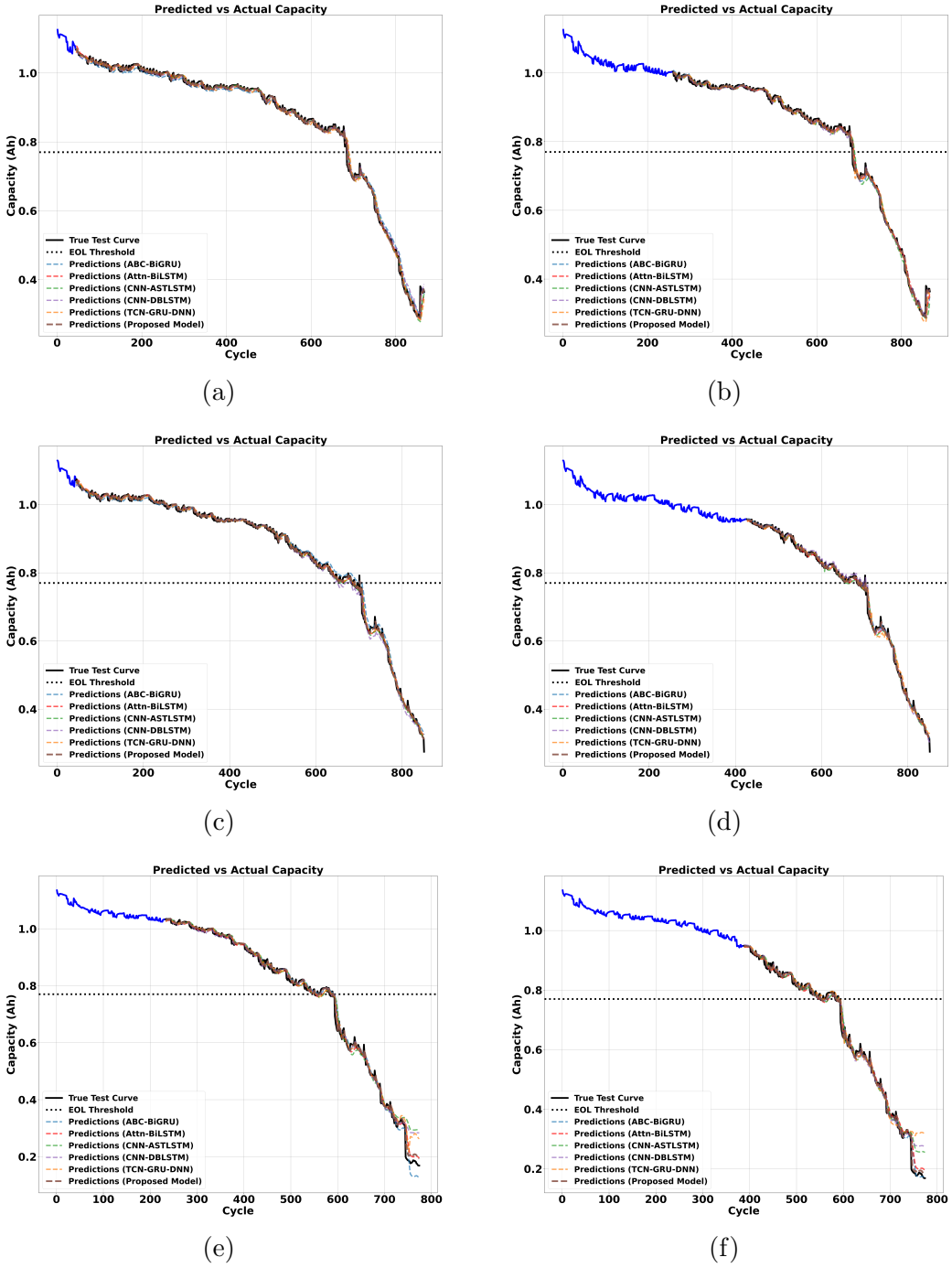

Figure 4.7: Degradation prediction scenarios in CALCE dataset (a) Scenario 4A (b) Scenario 4B (c) Scenario 5A (d) Scenario 5C (e) Scenario 6B (f) Scenario 6C.

4.3.4 Generalization and robustness of proposed model in SOH estimation

The various battery configurations for different experimental scenarios used in NASA and the CALCE are shown in Table 4.2. To ensure the robustness of the model,

different battery combinations with varying starting points are selected across multiple scenarios. Different batteries with different rated capacities are used in the NASA and CALCE datasets. The state-of-the-art algorithms include artificial bee colony-bidirectional GRU (ABC-BiGRU) [129], attention-bidirectional LSTM (BiLSTM) [151], TCN-GRU-deep neural networks (TCN-GRU-DNN) [152], CNN-active-state-tracking LSTM (CNN-ASTLSTM) [157], and CNN-deep bidirectional LSTM (CNN-DBLSTM) [158]. These state-of-the-art algorithms are selected based on papers that excel in the same NASA and CALCE datasets. The parameter configurations of the models are kept the same as those in the original papers, as these works have already been used in the same datasets employed in the proposed work for capacitance estimation. The proposed model strikes a balance with moderate memory requirements as well as reasonably fast inference time. The average training time is the mean time to train various battery configurations in multiple datasets for varying starting point conditions. The average inference time is the mean time required to predict battery state-of-health across various battery configurations and datasets under different starting point conditions. Similarly, the proposed models work in the NASA and CALCE datasets with excellent training efficiency, as shown in Table 4.3, faster than most alternatives with a moderate memory requirement.

The results across NASA and CALCE datasets as indicated in Table 4.4 and 4.5, show the proposed models' consistency in performance across different experimental scenarios. The proposed model performs better than the existing hybrid state-of-the-art algorithms in battery capacity degradation tasks with a lower MAE and RMSE value in almost all the experimental scenarios. The superior performance of MHDTCN-GRU in the case of an early prediction scenario indicated the robustness and accuracy of MHDTCN in estimating the degradation pattern of the battery. The proposed model performs better than the existing hybrid models across different starting point cases, showing its adaptability to varying prediction horizons. But in scenario 1-B, the CNN-

DBLSTM model has a lower MAE value of 0.0151 than the proposed model's 0.0160. The proposed model shows better performance across all other testing specifications, which reinforces its reliability and generalizability for various experimental conditions and dataset configurations. The graph showing the capacity degradation for NASA and CALCE datasets for various scenarios is given in Fig. 4.6 and Fig. 4.7, respectively. The proposed model achieves these results with parameter compatibility, making it a computationally efficient solution.

Table 4.4: Comparison of state-of-the-art methodologies on NASA dataset across different experimental scenarios.

M	Scenario 1A		Scenario 1B		Scenario 1C		Scenario 2A		Scenario 2B		Scenario 2C		Scenario 3A		Scenario 3B		Scenario 3C	
	MAE	RMSE	MAE	RMSE	MAE	RMSE	MAE	RMSE	MAE	RMSE	MAE	RMSE	MAE	RMSE	MAE	RMSE	MAE	RMSE
A	0.0278	0.0377	0.0177	0.0287	0.0175	0.0228	0.0204	0.0246	0.0084	0.0136	0.0075	0.0153	0.0331	0.0537	0.0289	0.0328	0.0251	0.0306
B	0.0157	0.0260	0.0202	0.0290	0.0152	0.0225	0.0079	0.0146	0.0065	0.0132	0.0108	0.0181	0.0234	0.0308	0.0181	0.0252	0.0191	0.0273
C	0.0174	0.0268	0.0197	0.0305	0.0145	0.0231	0.0086	0.0150	0.0086	0.0147	0.0116	0.0182	0.0329	0.0550	0.0244	0.0337	0.0278	0.0385
D	0.0182	0.0265	0.0287	0.0384	0.0186	0.0275	0.0101	0.0153	0.0127	0.0183	0.0127	0.0189	0.0276	0.0418	0.0280	0.0459	0.0180	0.0278
E	0.0182	0.0266	**0.0151**	0.0268	0.0127	0.0203	0.0146	0.0217	0.0075	0.0135	0.0078	0.0148	0.0507	0.0754	0.0285	0.0438	0.0267	0.0419
P	**0.0129**	**0.0223**	0.0160	**0.0252**	**0.0121**	**0.0201**	**0.0062**	**0.0121**	**0.0064**	**0.0126**	**0.0064**	**0.0144**	**0.0157**	**0.0244**	**0.0139**	**0.0211**	**0.0122**	**0.0218**

Note: In the above table, M - Model, A - ABC-BiGRU, B - Attention-BiLSTM, C - CNN-ASTLSTM, D - TCN-GRU-DNN, E - CNN-DBLSTM, P - **Proposed (MHDTCN-GRU)**

Table 4.5: Comparison of state-of-the-art methodologies on CALCE dataset across different experimental scenarios.

M	Scenario 4A		Scenario 4B		Scenario 4C		Scenario 5A		Scenario 5B		Scenario 5C		Scenario 6A		Scenario 6B		Scenario 6C	
	MAE	RMSE	MAE	RMSE	MAE	RMSE	MAE	RMSE	MAE	RMSE	MAE	RMSE	MAE	RMSE	MAE	RMSE	MAE	RMSE
A	0.0108	0.0142	0.0075	0.0119	0.0106	0.0156	0.0091	0.0131	0.0076	0.0106	0.0072	0.0102	0.0128	0.0263	0.0121	0.0185	0.0121	0.0183
B	0.0070	0.0107	0.0077	0.0119	0.0087	0.0140	0.0065	0.0092	0.0071	0.0100	0.0079	0.0111	0.0085	0.0135	0.0111	0.0172	0.0135	0.0199
C	0.0069	0.0107	0.0095	0.0152	0.0097	0.0154	0.0066	0.0092	0.0089	0.0131	0.0086	0.0120	0.0128	0.0279	0.0173	0.0327	0.0175	0.0294
D	0.0090	0.0137	0.0082	0.0123	0.0080	0.0118	0.0067	0.0090	0.0098	0.0130	0.0095	0.0133	0.0121	0.0199	0.0135	0.0243	0.0213	0.0415
E	0.0073	0.0104	0.0064	0.0090	0.0080	0.0108	0.0080	0.0111	0.0070	0.0094	0.0079	0.0108	0.0115	0.0239	0.0128	0.0272	0.0159	0.0300
P	**0.0044**	**0.0070**	**0.0050**	**0.0079**	**0.0054**	**0.0089**	**0.0044**	**0.0066**	**0.0051**	**0.0075**	**0.0056**	**0.0084**	**0.0069**	**0.0114**	**0.0079**	**0.0122**	**0.0081**	**0.0123**

Note: In the above table, M - Model, A - ABC-BiGRU, B - Attention-BiLSTM, C - CNN-ASTLSTM, D - TCN-GRU-DNN, E - CNN-DBLSTM, P - **Proposed (MHDTCN-GRU)**

4.4 Conclusion

This chapter presents a novel hybrid state of health (SOH) estimation model named multi-faceted temporal convolutional network with dynamic weight adaptation -gated recurrent unit (MFDWA-GRU) for addressing complex prolonged battery degradation scenarios. The achievement of this innovative hybrid model stems from the combination of multi-branch temporal convolutional networks with GRUs, enabling it to extract both multi-scale temporal patterns and the dynamic degradation behaviour of lithium-ion batteries. The model attains enhanced predictive accuracy across different battery configurations and operating conditions due to its adaptive weight updating features and attention blocks, which guide the model to essential features. The proposed model outperforms various state-of-the-art algorithms when tested against NASA and CALCE datasets across diverse experimental setups of the battery. MFDWA-GRU delivers improved mean absolute error (MAE) and root mean square error (RMSE) metrics across varied starting points, battery types, and prediction timeframes, demonstrating its broad applicability. The model also exhibits robust performance in early prediction scenarios, showcasing its practical potential for safety systems and battery management control. Incorporating Explainable Artificial Intelligence (XAI) methods, such as SHapley Additive exPlanations (SHAP), into the proposed model not only enhances predictive accuracy but also increases the transparency and interpretability of the prediction process.

Despite these achievements, LIBs represent only one part of the broader energy storage landscape. Many applications, especially those requiring rapid charge–discharge cycles, high power density, and extended service lifetimes, increasingly rely on supercapacitors as complementary or alternative storage devices. Both SOH and RUL are critical for assessing the reliability of energy storage devices; however, in the case of supercapacitors, accurate RUL estimation becomes particularly important due to their

frequent charge–discharge cycling and the need to ensure long-term operational stability. These requirements introduce unique modeling challenges, as the degradation behavior of supercapacitors differs significantly from that of batteries. Building upon the insights gained from SOH estimation in lithium-ion batteries, the next chapter shifts focus to RUL prediction in supercapacitors. To this end, a hybrid novel model is proposed, designed to capture multi-scale degradation patterns and sequential dependencies in supercapacitor aging data.